NEOPLASIA
www.neoplasia.com

Volume 23 Number xxx Month 2021 pp. 118–128

Bone marrow mesenchymal stem cells interact with head and neck squamous cell carcinoma cells to promote cancer progression and drug resistance ☆, ☆☆

Chuanxia Liu [a,b,c]; Sandrine Billet [b]; Diptiman Choudhury [b]; Ran Cheng [a,b]; Subhash Haldar [b]; Ana Fernandez [b,d]; Shea Biondi [b]; Zhenqiu Liu [b]; Hongmei Zhou [a,*]; Neil A. Bhowmick [b,d,*]

[a] State Key Laboratory of Oral Diseases, Department of Oral Medicine, West China Hospital of Stomatology, Sichuan University, Chengdu, Sichuan, China
[b] Department of Medicine, Cedars-Sinai Medical Center, Los Angeles, CA, USA
[c] The Affiliated Stomatology Hospital, Zhejiang University School of Medical, Hangzhou, China
[d] VA Greater Los Angeles Healthcare System, Los Angeles, CA, USA

Head and neck cancers are often diagnosed at later stages with poor outcomes. Mesenchymal stem cells (MSC) are recruited to primary tumor sites where they can have pro- and antitumorigenic influence. In trying to better understand the dynamics between MSC and cancer cells, we found that head and neck cancer-MSC exposure resulted in mesenchymal features, elevated proliferation rate, and were more motile, like the same cells that fused with MSC. We orthotopically grafted the parental head and neck cancer cells, those fused with MSC, or those exposed to MSC into the tongues of mice. The cancer cells originally incubated with MSC developed larger more aggressive tumors compared to the parental cell line. RNA sequencing analysis revealed the expression of genes associated with drug resistance in the cancer cells exposed to MSC compared to parental cancer cells. Strikingly, MSC exposed cancer cell lines developed paclitaxel resistance that could be maintained up to 30 d after the initial co-incubation period. The secretory profile of the MSC suggested IL-6 to be a potential mediator of epigenetic imprinting on the head and neck cancer cells. When the MSC-imprinted cancer cells were exposed to the demethylation agent, 5-aza-2'deoxycytidine, it restored the expression of the drug resistance genes to that of parental cells. This study demonstrated that the recognized recruitment of MSC to tumors could impart multiple protumorigenic properties including chemotherapy resistance like that observed in the relatively rare event of cancer/MSC cell fusion.

Neoplasia (2021) 23, 118–128

Keywords: Mesenchymal stem cells, Head and neck squamous cell carcinoma, Cell fusion, cancer progression, Drug resistance

Introduction

Head and neck cancer is the fifth most common type of cancer worldwide among all neoplasms, affecting more than 500,000 individuals each year. Head and neck squamous cell carcinoma (HNSCC) is the most common histological type with rising incidence worldwide. Approximately 40% of them occur in the oral cavity. Its pathogenesis is multifactorial but is mostly associated with cigarette smoke, alcohol, snuff, as well as papilloma virus, among others [1–3]. Currently tobacco and alcohol consumption are the major risk factors and seem to have a synergic effect [4]. Oral squamous cell carcinomas (OSCC) arise from the accumulation of genetic and epigenetic changes as well as abnormalities in cancer-associated signaling pathways. This includes limitless replicative potential, increased proliferation, ability to evade apoptosis, angiogenesis, invasion and metastasis. Drivers of OSCC include cyclin D1, p53, epidermal growth factor receptor, retinoblastoma, vascular endothelial growth factor receptor, and signal transducer and activator of transcription 3 [2,5].

The majority of OSCC are diagnosed at a late phase, in stages III or IV, which markedly decreases the chances of survival and leads to a significant deterioration in patient quality of life. Despite the currently available therapeutic strategies, which include the excision of malignant tissue in combination with radiotherapy and chemotherapy, the 5–yr survival rate is still around 50% [6–8]. In addition, a high percentage of patients have a poor response to therapy and high recurrence rates. In particular, tongue cancer is characterized by a massive potential for regional metastasis even in the early stages [9,10].

* Corresponding authors.
E-mail addresses: zhouhm@scu.edu.cn (H. Zhou), bhowmickn@cshs.org (N.A. Bhowmick).

☆ Funding: The work was supported by the Department of Veterans Affairs USA (I01BX001040) to NAB and the National Nature Science Foundation of China (No. 81772898) to HZ and China Scholarship Council to CL
☆☆ Conflict of interest: The authors declare no conflict of interest.
Received 8 October 2020; received in revised form 19 November 2020; accepted 25 November 2020

https://doi.org/10.1016/j.neo.2020.11.012

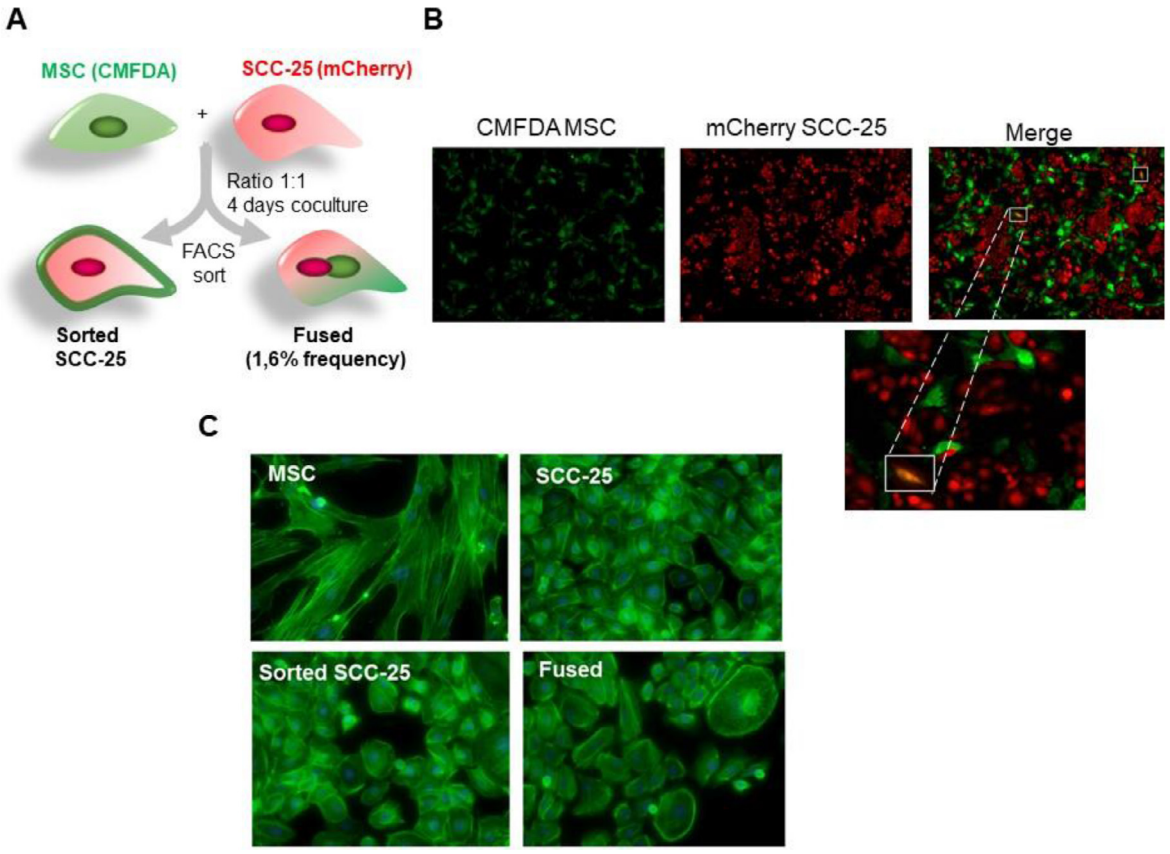

Figure 1. Co-culture of MSC cells and head and neck cancer cells influenced morphology of SCC-25 cancer cells. (A-B) Co-culture of green CMFDA-labeled MSC and mCherry-expressing SCC-25 at a 1:1 ratio for 4 days and observation under a fluorescent microscope. Spontaneous cell fusion was observed at very low rate (yellow cells). (C) Phalloidin staining of F-actin of the 4 cell types by immunofluorescence demonstrated a morphological change with the appearance of polynucleated cells (fused cells). MSC, Mesenchymal stem cells; SCC, squamous cell carcinoma. (Color version of figure is available online.)

Mesenchymal stem cells (MSCs), also called multipotent mesenchymal stromal cells, reside within the stromal compartment of most solid tissues and bone marrow space, are characterized to have multilineage differentiation potential [11,12]. Bone marrow MSC can differentiate into osteogenic, adipogenic, and chondrogenic lineages when placed in the appropriate environments. MSCs are also identified in various organs including those that occupy a perivascular niche [13–15]. MSCs express stromal fibroblastic markers (CD90, CD105, CD73) in the absence of hematopoietic markers (CD45, CD34, and CD14) and endothelial markers (CD31, CD34, vWF) [16,17]. MSCs tend to be recruited by injured tissues where they are thought to contribute to tissue repair, remodeling, and wound healing. As tumors are often considered to have characteristics of "injured tissues," MSCs are recruited to hypoxic tumor microenvironments. This property has brought MSC to the spotlight as potential therapeutic vehicles for anticancer drug/gene delivery [18,19].

MSCs can grow, proliferate, and transition into tumor-associated fibroblasts which ultimately promote tumor progression through their contribution in the microvascularization, stromal networks, and the production of tumor-stimulating paracrine factors [20,21]. Nevertheless, the role of tumor-associated MSC remains controversial with a number of studies showing that MSCs play an important role in tumor progression [22]. MSCs can migrate to the tumor site under a variety of cytokines and chemokines released from the tumor, such as SDF-1, VEGF-A, VCAM-1, HGF, and bFGF. MSC can evade the recognition of T cells and react with B cells, NK cells, and antigen-presenting cells. The immunosuppressive nature of MSCs favors tumor growth [23,24]. MSCs are primarily distributed in the tumor stroma after intravenous injection with a low frequency of hepatocellular carcinoma fusion [25]. Others have found that spontaneous cell fusion of bone marrow-derived MSC and breast cancer cells can promote the development of a more invasive/metastatic state [26]. However, fusion of human MSC with esophageal carcinoma cells declined cell growth, elevated apoptosis and reduced tumorigenicity [27]. While the differential effects of MSC fusion with cancer cells are primarily reported to favor a greater tumor-inductive state, the significantly more frequent association of the 2 cell types is less well characterized. In our present study, we investigated the effect of bone marrow-derived MSC recruitment to HNSCC tumors. We used human tongue SCC lines as models to establish how MSC impact cancer cell growth, metastasis, and chemotherapy sensitivity.

Results

Co-culture of bone marrow MSCs and head and neck cancer cells

To study the role of MSC on HNSCC we established co-cultures of human MSCs, derived from human bone marrow with SCC-25 cells at a ratio of 1:1. The MSC and the cancer cells were fluorescently tagged by a Green CMFDA cell tracker and by stable transfection with mCherry vector, respectfully (Figure 1A and B).

Spontaneous cell fusion was observed in the culture after the fourth day and mesenchymal morphological characteristics of binucleated yellow fluorescent hybrids cells had formed. However, this event was observed at very low frequency of 1.6%. These cells were then separated on a fluorescence basis

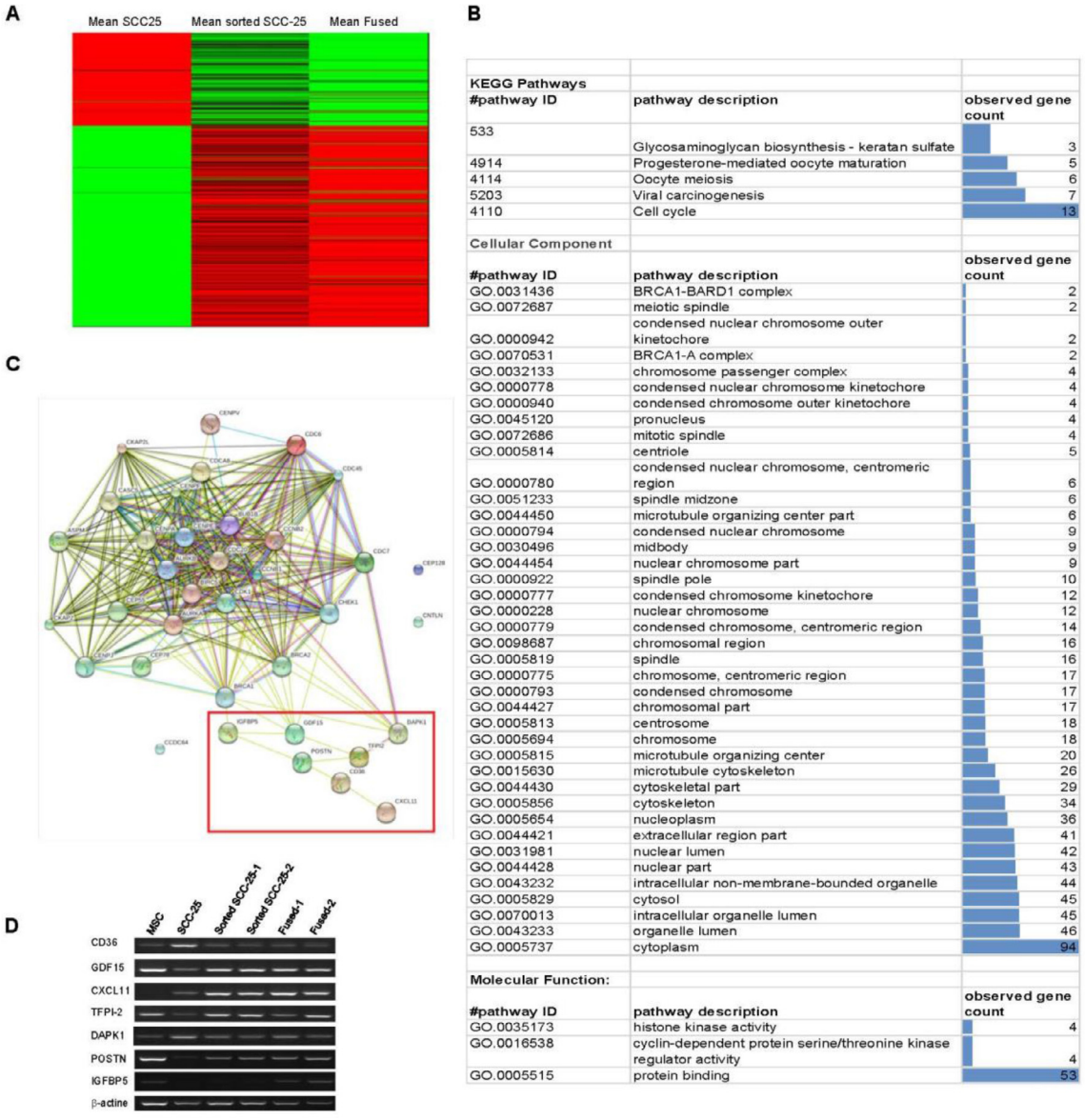

B

KEGG Pathways		
#pathway ID	pathway description	observed gene count
533	Glycosaminoglycan biosynthesis - keratan sulfate	3
4914	Progesterone-mediated oocyte maturation	5
4114	Oocyte meiosis	6
5203	Viral carcinogenesis	7
4110	Cell cycle	13
Cellular Component		
#pathway ID	pathway description	observed gene count
GO.0031436	BRCA1-BARD1 complex	2
GO.0072687	meiotic spindle	2
GO.0000942	condensed nuclear chromosome outer kinetochore	2
GO.0070531	BRCA1-A complex	2
GO.0032133	chromosome passenger complex	4
GO.0000778	condensed nuclear chromosome kinetochore	4
GO.0000940	condensed chromosome outer kinetochore	4
GO.0045120	pronucleus	4
GO.0072686	mitotic spindle	4
GO.0005814	centriole	5
GO.0000780	condensed nuclear chromosome, centromeric region	6
GO.0051233	spindle midzone	6
GO.0044450	microtubule organizing center part	6
GO.0000794	condensed nuclear chromosome	9
GO.0030496	midbody	9
GO.0044454	nuclear chromosome part	9
GO.0000922	spindle pole	10
GO.0000777	condensed chromosome kinetochore	12
GO.0000228	nuclear chromosome	12
GO.0000779	condensed chromosome, centromeric region	14
GO.0098687	chromosomal region	16
GO.0005819	spindle	16
GO.0000775	chromosome, centromeric region	17
GO.0000793	condensed chromosome	17
GO.0044427	chromosomal part	17
GO.0005813	centrosome	18
GO.0005694	chromosome	18
GO.0005815	microtubule organizing center	20
GO.0015630	microtubule cytoskeleton	26
GO.0044430	cytoskeletal part	29
GO.0005856	cytoskeleton	34
GO.0005654	nucleoplasm	36
GO.0044421	extracellular region part	41
GO.0031981	nuclear lumen	42
GO.0044428	nuclear part	43
GO.0043232	intracellular non-membrane-bounded organelle	44
GO.0005829	cytosol	45
GO.0070013	intracellular organelle lumen	45
GO.0043233	organelle lumen	46
GO.0005737	cytoplasm	94
Molecular Function:		
#pathway ID	pathway description	observed gene count
GO.0035173	histone kinase activity	4
GO.0016538	cyclin-dependent protein serine/threonine kinase regulator activity	4
GO.0005515	protein binding	53

Figure 2. Changes in gene expression of SCC-25 cancer cells with the effect of MSC. (A) Pattern of gene expression of sorted SCC-25 and fused MSC/SCC cells were compared to naïve SCC-25. Heatmap showing gene-level counts with lower than median (green), greater than median (red) and median (black) levels of expression. (B) Each row represents a single gene. (C) Network modeling of the interacting genes implicated mostly in drug resistance. (D) PCR of CD36, GDF15, CXCL11, TFPI-2, DAPK,1 POSTN, and IGFBP5 to validate genes obtained in the RNA-seq heatmap. MSC, Mesenchymal stem cells; SCC, squamous cell carcinoma. (Color version of figure is available online.)

by flow cytometry; green MSC, red SCC-25, and double fluorescent cells (fused SCC/MSC) and re-cultured individually for expansion. We cultured the MSCs, naïve SCC-25, the fused SCC/MSC cells and sorted SCC-25 on poly-L-lysine for morphology assessment. The sorted SCC-25 grew at a normal rate after 24 h of culture, where the adherent fused cells displayed either a SCC-25-like or MSC-like morphology. Nevertheless, the epithelial morphology was predominant with some larger multinucleated cells. Within 10 days, nearly all the cells were of epithelial morphology with distinct red fluorescence. The morphologic differences were better characterized by phalloidin staining for F-actin, where we identified the mesenchymal morphology of the MSC and certain sorted SCC had prominent stress fibers and little to no cortical actin. The epithelial morphology of the naïve SCC-25, majority of the sorted SCC-25, and even the fused SCC/MSC had prominent cortical actin staining with few stress fibers. Compared with spindle-shaped parental MSC cells, the co-cultured MSC cells gained a shorter more triangular shape.

To further evaluate whether MSC fusion or its proximity resulted in the observed increased mesenchymal morphology, we performed ribonucleic acid (RNA) sequencing for the 4 cell types. The gene expression profile was consistent with their derivatives from both parental partners, with 650 differentially expressed genes between SCC and sorted-SCC cells (Figure 2A and B). KEGG enrichment analysis revealed multiple differentially expressed microtubular and cytoskeletal genes (36) between SCC and sorted-SCC, in support of the observed structural changes in the sorted-SCC toward a more mesenchymal phenotype, reminiscent of an epithelial to mesenchymal transition (EMT)-like change (Figure 2C and Supplemental Figure S1).

There were added changes in cell cycle and biochemical pathways, highlighting genes implicated in drug resistance. Among the differentially

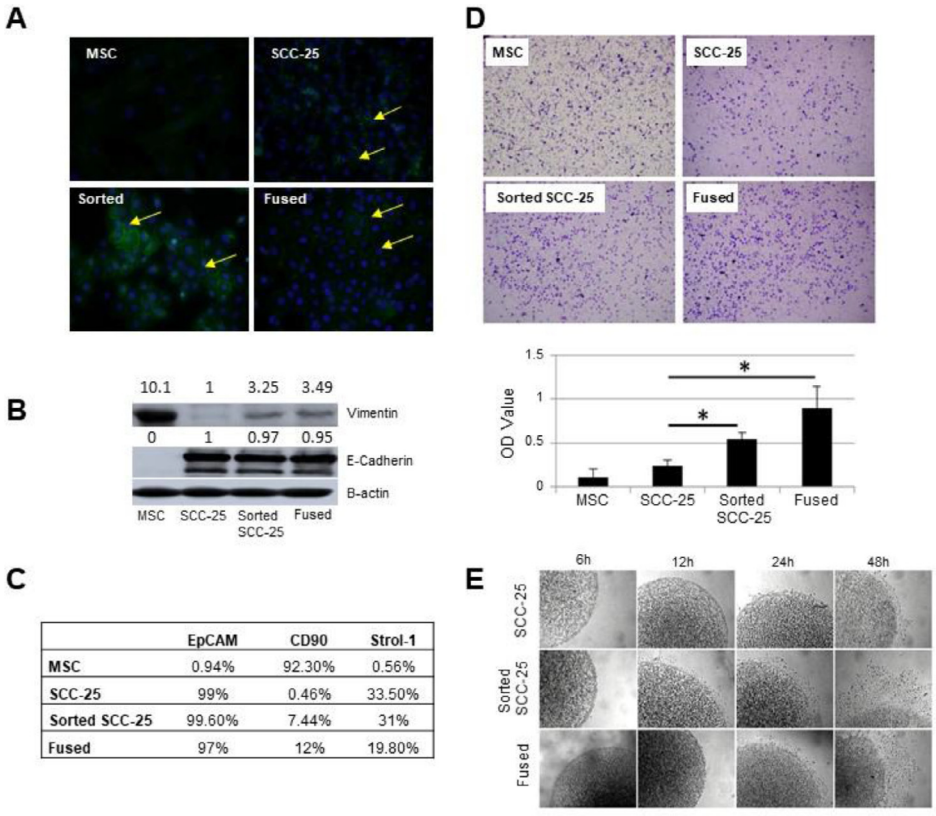

	EpCAM	CD90	Strol-1
MSC	0.94%	92.30%	0.56%
SCC-25	99%	0.46%	33.50%
Sorted SCC-25	99.60%	7.44%	31%
Fused	97%	12%	19.80%

Figure 3. Co-existence of MSC cells and head and neck cancer cells promoted EMT. (A) Immunofluorescence staining for ß-catenin in SCC-25, MSC, sorted-SCC and fused MSC/SCC cells demonstrated both plasma membrane and cytoplasmic localization. (B) Western blot analysis of EMT associated genes were evaluated for the expression of E-cadherin and vimentin. (C) Flow cytometry revealed epithelial EpCAM and mesenchymal CD90 expression. (D) Transwell migration assay showed differential mobility of naïve SCC, sorted-SCC and fused MSC/SCC cells. (E) Cell migration capacities of the 4 cell types seeded in collagen had differential rates of escape from the plugs was quantitated by light microscopy ($^*P < 0.05$). EMT, epithelial to mesenchymal transition; MSC, Mesenchymal stem cells; SCC, squamous cell carcinoma.

expressed genes, we observed POSTN, GDF11, IGFBP5, CXCL11 upregulated, and DAPK1 downregulated in the sorted-SCC exposed to MSC and MSC/SCC fused cells, compared to the naïve SCC. These RNA sequencing findings were validated by reverse transcriptase polymerase chain reaction (rtPCR) to be consistent with markers of poor prognosis (Figure 2D).

MSC-induced transdifferentiation of SCC-25

The morphological and gene expression changes suggested MSC fused and sorted SCC-25 exposed to MSC underwent EMT. To this end, immunofluorescence detection of β-catenin protein at the plasma membrane was absent in the MSC and sorted-SCC-25 with positive staining in the cytoplasm and nucleus. Both the SCC-25 and MSC/SCC fused cells expressed β-catenin at the plasma membrane (Figure 3A).

Additional western blotting for E-cadherin in the sorted SCC-25 and MSC/SCC fused cells had similarly high levels to naïve SCC-25 with co-expression of vimentin sorted SCC-25 and MSC/SCC fused cells (Figure 3B). Characterization on these cells was also performed by flow cytometry analysis of typical epithelial marker, EpCAM, as well as a typical mesenchymal surface marker, CD90 (Figure 3C). Sorted SCC-25 and MSC/SCC fused cells had a similar EpCAM expression levels as SCC-25 cells (approaching 100%), whereas MSC had negligible expression. However, the sorted SCC-25 and fused cells has similar expression of CD90, like MSC. Together, examining the classic markers of EMT would suggest that the SCC exposure to MSC resulted in a mixed differentiated status.

Cell motility was measured using the transwell migration assay and a collagen evasion assay. After plating cells in the transwell chambers the cells were allowed to migrate for 6 h and visualized following crystal violet staining. The sorted-SCC-25 exposed to MSC and MSC/SCC fused cells had significantly greater migratory capacity compared to naïve SCC-25 ($n = 5$, Figure 3D). The collagen evasion assay where equal number of cells were seed in collagen supported the same conclusion as the migration assay ($n = 20$, Figure 3E). The results showed that SCC-25 and fused cells similarly escaped the collagen plug and migrated on the dish significantly more than the naïve SCC-25 cells. While EMT marker expression was equivocal in the MSC/SCC fused and sorted-SCC cells, they similarly demonstrated greater motility compared to naïve SCC, in support of the concept that recruitment of MSC to tumors can promote tumor migration regardless of the low frequency fusion events.

MSC-induced proliferation of SCC-25

Characterization of these cells was further explored on a functional aspect, by evaluating their viability. The result showed that sorted-SCC-25 and fused cells proliferated about 2-fold faster than the parental naïve SCC cells and that growth ($P < 0.001$; Figure 4A).

However, flow cytometry of propidium iodide stained cells revealed an elevated number of sorted-SCC in S phase compared to naïve SCC-25 or MSC/SCC fused cells (Figure 4B). Predictably, the fused SCC/MSC maintained elevated levels of aneuploidy and polyploidy by propidium

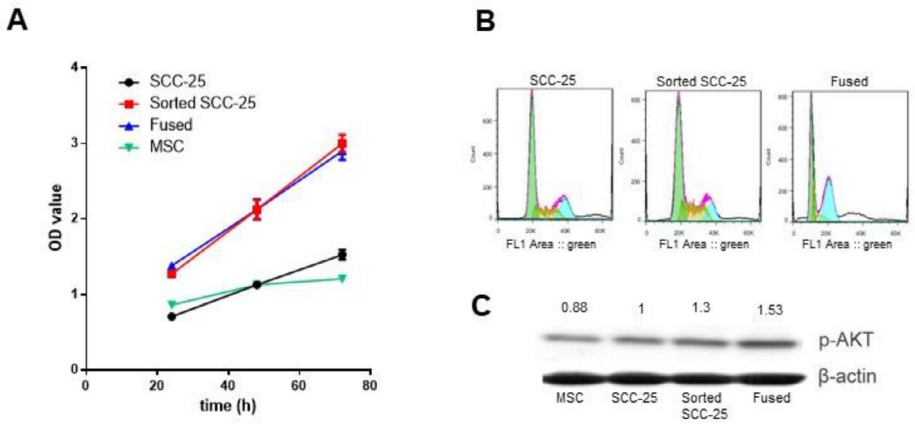

Figure 4. Effect of MSC co-culture or fusion on proliferation and cell cycle of SCC-25 cancer cells in vitro. (A) MTT assay evaluating cell proliferation of SCC-25, MSC, sorted SCC-25 and fused MSC/SCC cells at 24, 48, and 72 h ($P < 0.001$ compared to SCC-25). (B) Cell cycle analysis was performed in 4 cell types by flow cytometry following propidium iodine staining for cell cycle determination. (C) Proliferation pathway evaluated by Akt phosphorylation by western blot in the studied cell types. MSC, Mesenchymal stem cells; SCC, squamous cell carcinoma.

iodide stained fluorescent assisted cell sorting (FACS) analysis. The PI3K/PTEN/AKT signaling cascade plays a critical role in the transmission of signals from growth factor receptors to regulate gene expression and prevent apoptosis. Components of this pathway are mutated or aberrantly expressed in human cancers, playing critical roles in promoting cancer growth. In this study, we tested phosphorylated-AKT expression by western blot in the 4 cell types, to find that there was elevated AKT activation in sorted-SCC and fused cells in comparison to either the naïve SCC-25 cells or MSC (Figure 4C). Thus, despite the similarities in proliferative status of the MSC/SCC fused and MSC exposed sorted SCC-25 cells, the sorted SCC-25 uniquely increased proliferation associated with elevated PI3K signaling.

The role of bone marrow-derived MSC on tumor progression and chemotherapy resistance

To confirm the migration capacities of these cells in a more physiological setting, mimicking stromal and epithelial interaction in tumors, we generated 3D cell cultures of the four cell types in Matrigel/collagen matrix [28,29]. The spheroid cultures of the sorted SCC-25 and MSC/SCC fused cells were found to sprout into processes that extended from the core cell cluster, an indication of an invasion behavior. Conversely, the naïve SCC-25 cells maintained a spheroid morphology (Figure 5A).

To investigate whether these cells could promote cancer expansion *in vivo*, we used the 4 cell types to establish an orthotopic xenograft tumor models in mouse tongues (Figure 5B). The tongue tumors were allowed to grow for 4 wk in Nude mice. Histological evaluation of the tissue sections illustrated a more aggressive pattern for the sorted-SCC and MSC/SCC fused cells, compared to the naïve SCC-25 cells. It was not surprising that the MSC/SCC fused cells developed larger tumors with an uneven invasive front. We also found that exposure of SCC-25 cells to MSC rendered the tumors more proliferative, based on the significantly greater Ki-67 staining with a ragged invasive front. These observations in the mice were consistent with the culture models.

In the light of the evidence in support of EMT in the sorted-SCC described and the reported impact of EMT on chemotherapy sensitivity, we examined if such changes were imparted on SCC by MSC exposure [30]. The specific differentially expressed genes (i.e., GDF15, CXCL11, TFPI-2, POSTN, IGFBP5, CD36, and DAPK1) in the sorted-SCC have been implicated in cancer drug resistance. For the next set of experiments to determine the role of MSC on chemosensitivity we selected paclitaxel, as the cytotoxic chemotherapeutic as it is the standard of care for several solid tumors including those of squamous tongue type like SCC-25. Dose response curves for paclitaxel revealed naïve SCC-25 cells to be significantly more sensitive, compared to the sorted-SCC and the MSC/SCC fused cells ($P < 0.01$; Figure 6A).

The IC_{50} for the sorted-SCC was comparable to the MSC/SCC fused cells at over a log paclitaxel concentration greater than that for the naïve SCC-25 cells. Consistent with a protective effect of the MSC on cancer cells regarding drug-induced apoptosis [31,32], we observed a significantly lower expression of cleaved-caspase 3 and cleaved-PARP-1 by the sorted-SCC and MSC/SCC fused cells, compared to naïve SCC-25 by western blotting in a time dependent manner with paclitaxel treatment. The longer the cells were exposed to the paclitaxel the greater the difference in apoptosis markers were visible among the cell types with a maximal effect observed at 48 h. These findings were consistent with the elevated BCL2 expression by the sorted-SCC and MSC/SCC fused cells (Figure 6B). The genes originally identified by RNA sequencing incidentally have also been implicated in drug resistance, (*e.g.,* GDF15, CXCL11, TFPI-2, POSTN, IGFBP5, and DAPK1) were differentially expressed in the naïve SCC-25, MSC/SCC fused and sorted SCC-25. Accordingly, mice grafted with naïve- and sorted-SCC were grafted into mice and administered paclitaxel. It was evident that the sorted-SCC were more resistant to paclitaxel compared to naïve SCC-25 based on the difference in tumor size (Supplemental Figure S1).

The specificity of cell-cell interaction was interrogated by titrating the ratio of MSC and SCC-25 to evaluate the durability of the MSC effects on the SCC-25. The MCS capacity for SCC-25 conversion to a chemoresistant state was measured through the expression of the resistance gene panel. The MSC and SCC-25 were mixed at a ratio from 1:1 to 1:10, respectively. We found that POSTN, ABCG, and MRP1 were upregulated in the sorted-SCC, compared to the naïve SCC-25 cells at ratios of MSC:SCC-25 of 1:10 (Figure 7A).

At the 1:10 proportion of MSC:SCC-25, the expression of POSTN, ABCG, and MRP1 by sorted-SCC was similar to MSC/SCC fused cells. To determine the stability and duration of the acquired chemoresistance of sorted-SCC cells, dose-response curves with paclitaxel were compared for 3 to 30 days following co-incubation with MSC (Figure 7B). The MSC effect on the drug resistance of sorted-SCC cells lasted as long as 30 d with a maximum effect after 3 d of MSC exposure ($IC_{50} = 2.02$ compared to parental SCC-25 $IC_{50} = 1.4$; $P < 0.0001$), that was maintained significantly for 7 ($IC_{50} = 1.9$, $P < 0.005$) and 15 days ($IC_{50} = 1.8$, $P < 0.05$). There was a lesser effect

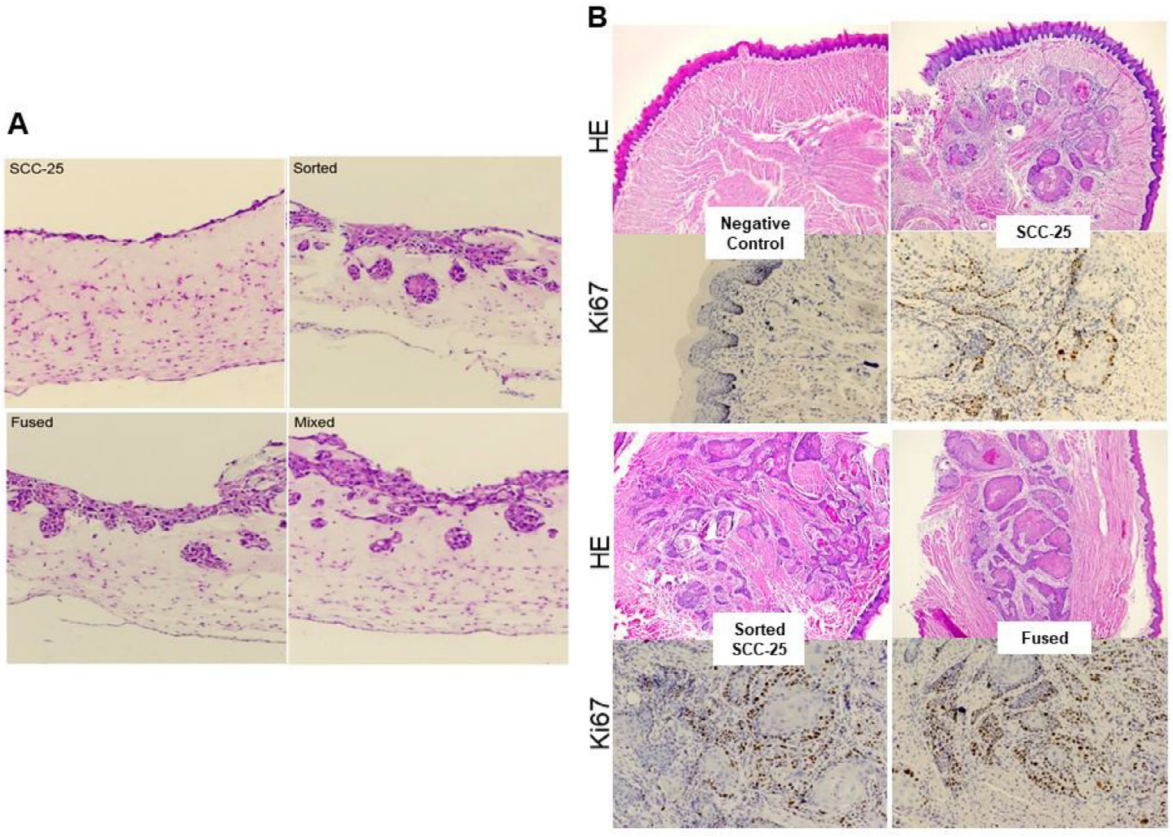

Figure 5. MSC cells promoted invasion and tumor growth. (A) 3D cultures of naïve SCC-25, sorted SCC-25 and fused MSC/SCC cell in Matrigel/collagen allowing the cells to present a spheroidal morphology indicating invasion capacity was visualized by H&E. (B) Naïve SCC-25, sorted SCC-25, and fused MSC/SCC cell were injected in nude mice. Presented H&E and Ki67 IHC histological stains of the tumor observed in the tongue. MSC, Mesenchymal stem cells; SCC, squamous cell carcinoma.

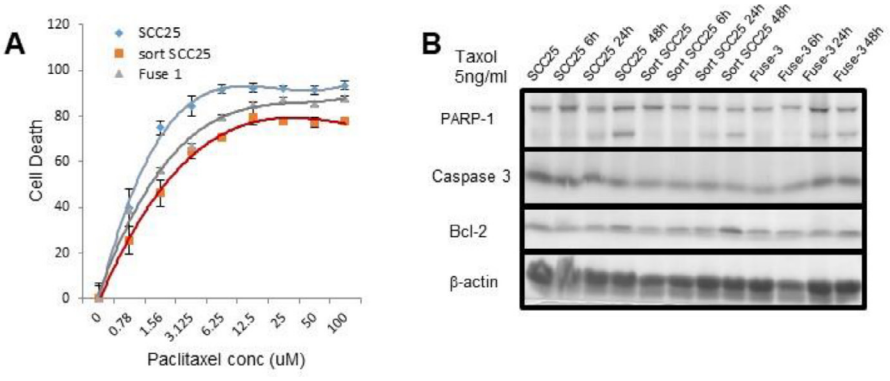

Figure 6. *Co-existence of MSC cells and head and neck cancer cells promoted drug resistance.* (A) Sensitivity of parental SCC-25 to paclitaxel compared to sorted-SCC and fused MSC/SCC cells observed in a dose dependent manner a protective effect of MSC presence or fusion ($P < 0.01$). (B) Apoptotic pathway was evaluated by western blot after time dependent treatments with paclitaxel of the different cell types. MSC, Mesenchymal stem cells; SCC, squamous cell carcinoma.

with MSC exposure to HSC-2 cells having a significant difference compared to the parental HSC-2 up to 7 d ($IC_{50} = 15.35$ compared to IC_{50} 12.7 for parental HSC-2; $P < 0.01$). Since the drug resistance memory was imparted merely by the proximity to MSC, we performed a human cytokine array to determine the secretory status of the lines to find that IL-6 to be the most elevated cytokine in the co-cultured cells (Figure 7C and Supplemental Figure S2). As IL-6 is known for its capacity to regulate DNA methylation, we subjected these cells to 5-aza-2′-deoxycytidine (5-azaDC), a DNA methyl transferase inhibitor. We observed an elevated expression of ABCG, MDR1, MRP1, and POSTN by the naïve SCC-25 cells, compared to sorted-SCC cells by western blot following 5-azaDC treatment (Figure 7D). Together, the effects of bone marrow-derived MSC proximity to SCC were revealed to impact morphology, cell expansion, invasive capacity, and a lasting resistance to chemotherapy (Figure 8).

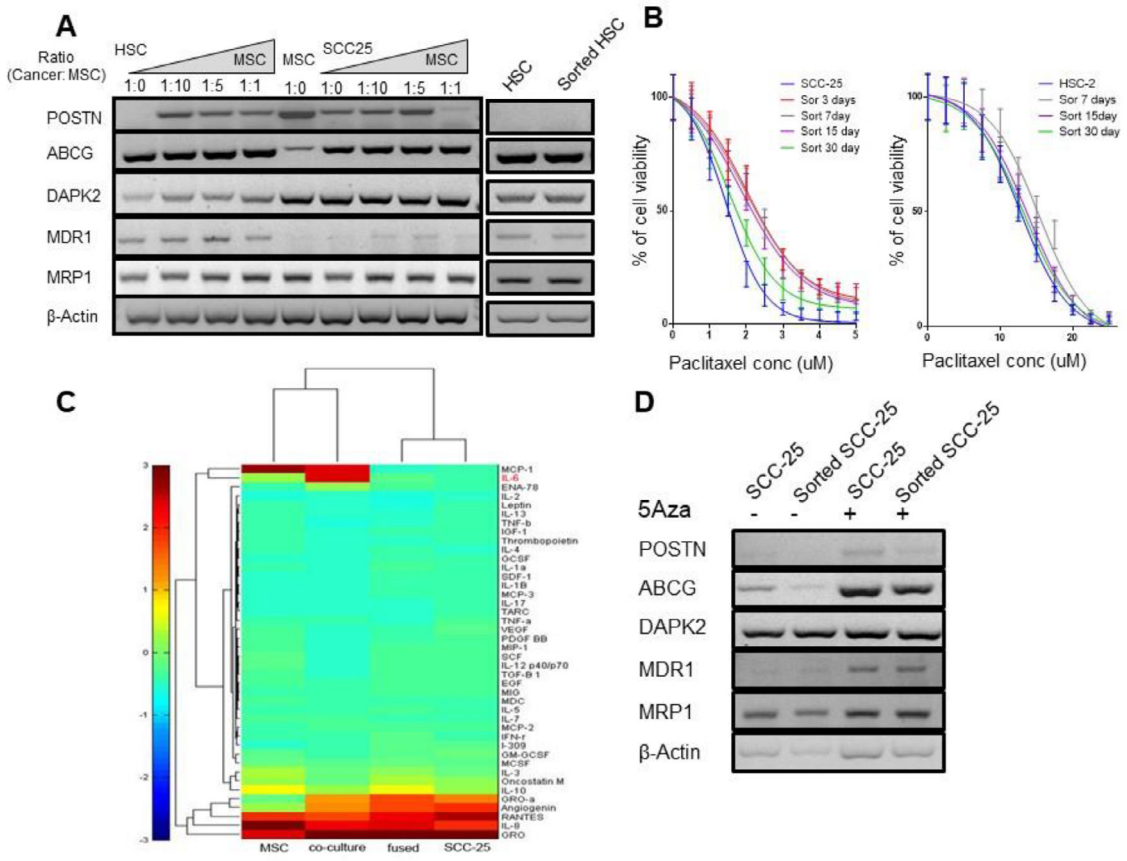

Figure 7. *Co-existence of MSC cells and head and neck cancer cells promoted drug resistance and memory through epigenetic modifications*. (A) Gene expression of POSTN, ABCG, DAPK2, MDR1, and MRP1 on SCC-25 and associated MSC and cancer cells at different ratios from 1:1 to 1:10. (B) Cell viability analysis of 30 days. The results showed that co-existence of MSC cells and head and neck cancer cells promoted drug resistance and memory for SCC-25 cells with an effect up to 15 days ($P< 0.0001$ to 0.05) and HSC-2 with an effect for 7 days ($P < 0.01$). (C) Heat map resulted from a human cytokine array of the 4 cell types demonstrated differential IL-6 expression. (D) 5-AzaDC mediated changes in genes associated with drug resistance comparing SCC-25 and sorted SCC-25. MSC, Mesenchymal stem cells; SCC, squamous cell carcinoma.

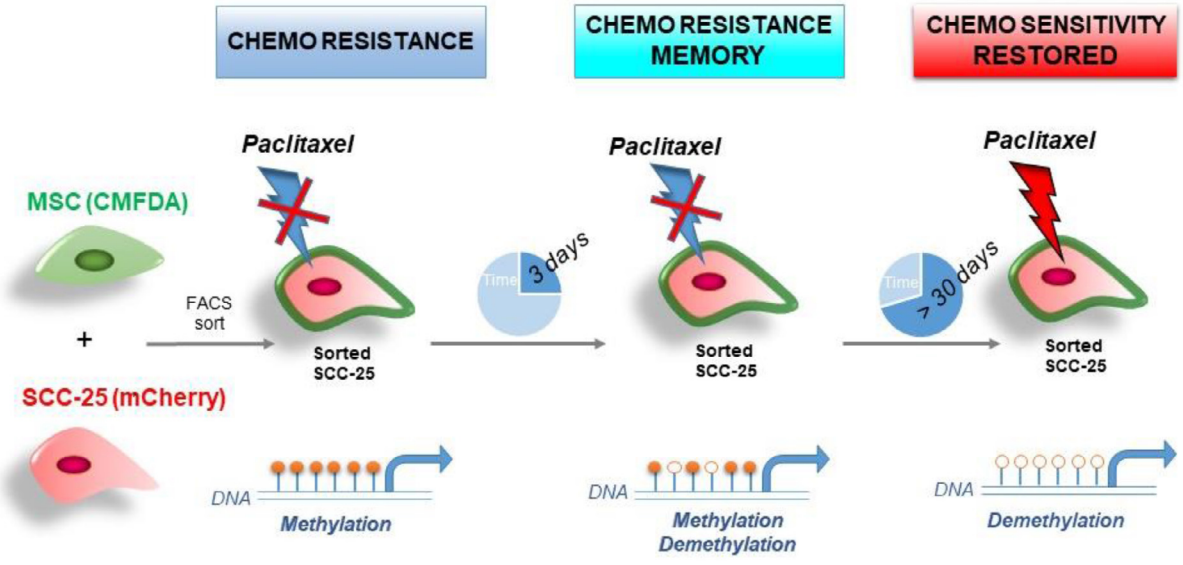

Figure 8. *Model of the MSC-induced phenotype on SCC-25*. The proximity of MSC and head and neck cancer cells can mediate paclitaxel resistant and this resistance can be maintained through epigenetic modifications up to 30 days. MSC, Mesenchymal stem cells; SCC, squamous cell carcinoma.

Discussion

Bone marrow-derived stromal cells such as MSCs infiltrate solid tumors. Much has been reported on the role of MSC on promoting tumor progression as well as its potential application as a means of delivering anticancer agents based on their reliable tumor recruitment and fusion with cancer cells [33–35]. The 2 methods by which MSC can influence cancer progression include the direct fusion with cancer epithelia and via paracrine signaling impacting the proximal cancer and immune cells [36,37]. The relatively rare event of cancer cell fusion with MSC as well as leukocytes are recognized as a protumorigenic event that contributes to tumor heterogeneity [38,39]. We investigated the effect of the co-existence of bone marrow MSCs with head and neck cancer models compared to that of naïve and cancer cell/MSC fusion. Our experiments demonstrated that bone marrow-derived MSCs promoted the proliferation, invasion, tumorigenicity, and paclitaxel resistance of HSC-2 cells (Figure 8). The role of carcinoma associated fibroblasts in the support and promotion of tumor progression is well documented [40–43]. However, the origin of carcinoma associated fibroblasts can include bone marrow-derived MSC, expansion of resident fibroblasts, or EMT. Although MSCs have been reported in the progression of head and neck cancer cells [44], the underlying mechanisms remain underexplored. Therefore, we further investigated the interaction of MSC with head and neck cancer cell lines and the associated mechanisms in this study.

EMT is the usual process during wound healing and organ fibrosis in which epithelial cells undergo morphological changes that result in increased cell plasticity and mobility as they transition into a mesenchymal-like cell phenotype. EMT can be also observed in a variety of cancer tissues. In human head and neck cancer, EMT is often detected at invasive lesions and tumor peripheries at the interface between cancer cells and host cells surrounded by extracellular matrix. MSCs have been reported to promote the expression of an EMT phenotype in several cancer cell types [45–47]. In the present study, we demonstrated that direct contact between cancer cells and MSCs can support an EMT status that involve both the expression of ß-catenin at the plasma membrane as well as vimentin, all the while promoting cell motility.

Our results revealed that MSC promoted the proliferation and affect cell cycle of SCC-25 cancer cells. The MTT, Ki67, and BrdU staining assays demonstrated that MSC conditioned media significantly enhanced the proliferation of cancer cell lines. To further support the tumor promoting effect of MSC, these modified cancer cells were injected in the tongue of nude mice to establish xenograft tumor models. Likewise, Jung Y et al found that the recruitment of MSC into prostate tumors promoted tumor metastasis [48]. Further, human bone marrow MSC induce tongue cancer invasion [49]. De Boeck et al found that MSC promoted colorectal cancer progression through paracrine neuregulin 1/HER3 signaling [50]. Together, these observations indicated that bone marrow MSC promoted the invasion and tumor growth of head and neck cancer.

Our results revealed that the morphology and biological characteristics of SCC-25 could be changed when co-cultured or fused with MSC. These findings are especially relevant, as MSCs enrichment in head neck squamous cell carcinoma has been correlated increased tumor size and inhibition of T-cell proliferation [36]. Previously, bone marrow-derived MSC fusion was observed in the processes of prostate epithelial regrowth following restoration of androgen signaling and hepatocellular carcinoma expansion [25,28]. Here we analyzed the gene expression pattern of SCC-25 cancer cells in response to MSC fusion as well as its association. The striking number of overlapping genes in the cancer cells fused and sorted from recent association with MSC seemed to be primarily cytoskeletal and nuclear lumen proteins. Interestingly, we identified a number of stem genes common to the fused and sorted cancer cells as well.

MSC recruited to tumors as part of its microenvironment have been demonstrated to increase drug resistance [51,52]. The stem genes elevated in cancer cells by MSC association or fusion was consistent with this model. For example, MSC-derived exosomes induced expression of the stem marker, CD133, by gastric cancer cells to similarly support chemotherapy resistance [53,54]. While we have not ruled out the role of exosomes in our current study, we found that the presence of MSC supported the resistance of head and neck cancer lines (i.e., SCC-25 and HSC-2) to paclitaxel by an epigenetic manner potentially induced by paracrine IL-6 expression. MSC in the microenvironment can influence tumor progression, drug resistance, and a target for cancer treatment.

Materials and methods

Cell culture

Human MSCs were obtained from Lonza (Morristown, NJ, USA). These cells were characterized both through standard surface markers and functional analysis. The cells were validated to express CD29, CD44, CD105, CD90, and CD166 and to not express CD14, CD34, CD19, and CD45. The cells were tested to differentiate down each of the 3 lineages (adipogenic, chondrogenic, osteogenic). The cells were cultured in α-modified Eagle's medium supplemented with 10% Hyclone fetal bovine serum, 100 units/mL penicillin and 100 μg/mL streptomycin (all from Fisher Scientific Waltham, MA, USA) at 37°C in a humidified 5% CO_2 atmosphere for $\leq$6 passages. The human SCC-25 cell lines (ATCC, Manassas, VA, USA) were cultured in Dulbecco's modified Eagle's medium (Fisher Scientific) supplemented with 10% FBS, 100 units/mL penicillin and 100 μg/mL streptomycin at 37°C in a humidified 5% CO_2 atmosphere.

Fluorescent labeling of MSC and SCC-25

Cell Tracker Green (CMFDA, Invitrogen, Carlsbad, CA, USA) was used to label MSC cells seeded in 100-mm cell culture dish, when they reached 70% confluency. The cells were washed 3 times with phosphate buffered saline (PBS), incubated 2 × 30 min at 37 °C with 2-μM Cell Tracker dye, and washed subsequently 3 × with PBS. MCherry plasmid DNA (TaKaRa Bio, Mountain View, CA, USA) was used to label SCC-25 cells. This plasmid was transfected by electroporation using Amaxa Cell Line Nucleofector Kit according to manufacturer protocol (Lonza). The cells were then seeded on poly-L-Lysine precoated plates and fluorescence intensity was evaluated under a fluorescent microscope (Olympus Waltham, MA, USA). G418 was used as a selection antibiotic for stable expression of mCherry in SCC-25 cells.

Co-culture of MSC and SCC 25 in vitro

Green fluorescent MSC and mCherry SCC-25 cells were counted, mixed at a ratio of 1:1, and plated in a 100mm cell culture dish. After co-culturing of green MSC and mCherry SCC-25 fluorescent cells for 4 d a few cells could be observed to have spontaneously fused. The fused SCC/MSC (green and red) and sorted-SCC (red) cells were segregated by FACS. Each cell was then cultured separately.

Cell viability assays

MTT assay was used to detect the viability of each cell type by manufacturer's guidelines (Sigma, USA). Briefly 2×10^4 cells were counted and seeded in 96-well plate, 5 mg/mL MTT solution (3-(4,5-Dimethylthiazol-2-yl)-2,5-diphenyltetrazolium bromide) was added in each well and incubated for 4 h at 37°C at 24, 48, and 72 h time points. MTT solution was replaced by dimethyl sulfoxide (DMSO) and absorbance was measured at 490 nm using a μQuant plate reader (Thermo Varioskan Flash, MA, USA).

FACS analysis

FACS experiments were performed with eBiosciences (San Diego, CA USA) antibodies: anti EpCAM, anti-human CD90 and anti-human Stro-1 following standard protocol. All events were acquired on LSR II flow cytometry (Becton, Dickinson, Franklin Lakes, NJ) and files were analyzed using Flow-Jo software v10.3. Cell cycle status was evaluated following fixation of 1×10^6 cells in ice-cold 70% ethanol then incubated in 10 μg/mL propidium iodide solution containing 200 μg/mL RNase A. For each experiment, 10,000 events were evaluated by FACS analysis and cell cycle profiles were modeled using FlowJo software.

Motility/invasion assays

Transwell assay was used to detect the migration ability of parental SCC-25, sorted SCC-25 and fused SCC/MSC. 5×10^4 cells were resuspended in 100 µL serum-free medium and inoculated into the upper transwell chamber, and 400 µL complete medium with 10% FBS was put in the lower chamber. After 6 h of culture, the cells have migrated toward the lower side of the membrane, they were fixed by 100% methanol, washed with PBS, and stained with 0.1% crystal violet solution. The nonmigrating cells were removed from the upper side of the chamber with a swab allowing the migrated cells to be counted under a microscope.

1×10^6 SCC-25, sorted SCC-25 and fused MSC/SCC cells were prepared in 1 mL collagen I and neutralized by setting solution. The cell suspensions were then seeded 1 μL per spot for each cell type with 20 replicates per cell type. After the collagen culture was solidified medium containing 5% FBS was added to the dish. The collagen grafts were imaged by phase contrast light microscope after 6, 12, 24, and 48 h of culture.

3D cell culture

Three-D cell culture was used to confirm the migration capacity of the cell types. Briefly, on day 1: the basement gels were prepared using 3.5 volumes of type I collagen and 3.5 volumes of Matrigel, with 1 volume of 10 × DMEM, 1 volume of FBS and 1 volume of medium. 300 µL of this mixture was pipetted into each well of a 48-well plate and allowed to solidify prior to adding 1 mL of medium to each well for equilibration. On day 2: 2×10^5 SCC-25, sorted SCC-25, or fused MSC/SCC cells were seeded on the gel after the medium was aspirated from the wells. On day 3, after the cells settled on the gels, they were placed on collagen-coated nylon sheets supported on metal grids to limit lateral contraction of the gel. The medium covering the gels was carefully aspirated without disturbing the surface of the gels, thus allowing the gels to be removed from the 48-well plate and placed onto individual collagen-coated nylon discs resting on the steel using a sterile spatula in 6 well plates. Then 2 mL growth medium was added to each well to reach the undersurface of the grid. The medium was changed every 2 d. After 14 d, the 3D cultures were harvested and histopathologically processed for imaging.

Immunofluorescence

Phalloidin staining of F-actin was done by immunofluorescence. Briefly, MSC, SCC-25, sorted SCC-25 and fused cells were seeded onto glass slides in 6 well plates. After 24 h, the cells, at about 50% confluence were fixed by paraformaldehyde (4%). After the slides were washed three times with PBS, they were blocked with 5% normal goat serum in PBS for 1 h at room temperature. Fluorescein-conjugated phalloidin (Sigma) was incubated for 10 min at room temperature, then washed again 3 times with PBS prior to being counterstained with 4,6-diamidino-2-phenylindole for 2 min. After 3 more washes, cover glass was placed with antifade mounting medium for imaging.

Western blot analysis

MSC, SCC-25, sorted SCC-25 and fused MSC/SCC cells were seeded at 5×10^5 cells/dish in 100-mm cell culture dishes. Cell lysates (20 μg) were electrophoresed and transferred to polyvinylidene fluoride (PVDF) membranes for probing for p-AKT (Cell Signaling Technology, Danvers, MA USA), p-STAT3 (Cell Signaling Technology), β-actin antibody (Santa Cruz Biotechnology, Santa Cruz, CA, USA), E-cadherin (Cell Signaling Technology), vimentin (Santa Cruz Biotechnology), PARP1 (Santa Cruz Biotechnology), capase-3 (Cell Signaling Technology), and Bcl2 (Cell Signaling Technology). Western blots were visualized using alkaline phosphatase-conjugated secondary antibodies (Sigma-Aldrich, St Louis MO, USA).

Animal experimental procedure

Animal studies were carried out in accordance with Institutional Animal Care and Use Committee approved protocol. All surgeries were performed under anesthesia. The xenograft experiment was implemented in male BALB/c nude mice (about 4 wk old). The mice were randomly divided into 3 groups with 10 mice in each group. SCC-25, sorted SCC-25 or fused MSC/SCC 5×10^5 cells were prepared in 30 µL type I collagen solution injected into the middle tongue of the mouse. Two weeks after injection, tumors could be visualized, and mice were harvested 4 wk after injection. The tumors were fixed with 4% paraformaldehyde. H&E and Ki67 staining were accomplish by IHC.

Immunohistochemical analyses

Ki67 staining was done by immunochemistry (Abcam, Cambridge, UK). Briefly, paraffin-embedded sections were deparaffinized in xylene, rehydrated through graded ethanols, and then submerged into citric acid buffer for heat-induced antigenic retrieval, blocked with 10% bovine serum albumin, incubated with Ki67 primary antibodies at 4°C overnight and developed using the DAKO ChemMate Envision Kit HRP (Dako-Cytomation, Carpinteria, CA, USA) followed by counterstaining with hematoxylin, dehydration, clearing and mounting.

RT-PC

To confirm and validate data obtained by the RNA-Seq, DNA was extracted with a RNA Easy Qiagen kit following manufacturer's protocol. The sequence of the primers are detailed in Supplemental Table 1.

Human cytokine array

Human cytokine arrays (Ray Biotech Inc, Norcross, GA, USA) consists of a total of 120 different cytokines and chemokines antibodies spotted on a membrane to detect the cytokine secretion profile of MSC, SCC-25, fused cells and the co-culture cells of MSC and SCC-25. First, conditional medium was prepared. Total numbers of 1×10^6 cells were seeded on 100-mm dish. After 24 h, cells were washed 3 times with 10 mL PBS and incubated for another 48 h at 37°C in 10 mL α-MEM medium without fetal bovine serum. The medium was harvested and centrifuged at 1000 rpm for 10 min at 4°C and the supernatant was stored at −80°C. Control medium was collected in parallel from tissue culture dish containing no cells. The proteins secreted were then evaluated according to the manufacturer's instruction. Briefly, protein array membranes incubated in blocking buffer for 30 min and then incubated with conditioned media at 4°C overnight. After being washed, membranes were incubated with biotin-conjugated antibodies at room temperature for 2 h and then visualized after incubation with horseradish peroxidase-conjugated streptavidin (1:1000 dilution). The signal

intensities were quantified by densitometry and fold changes in protein expression were calculated.

Statistical analysis

Data analysis was performed using SPSS 13.0 statistical software. Comparison between 2 groups were performed by unpaired Student *t* test, while multiple group comparison was performed by 2-way ANOVA using Prism Stat view software. All tests were 2-sided and *P*values <0.05 was considered to be significant.

For the RNA-seq data, raw sequencer data was processed using Illumina's RTA and CASAVA pipeline software, which includes image analysis, base calling, and sequence quality scoring. Moreover, we analyzed the RNA-seq data with our transcriptome analysis pipeline, which uses the TOPHAT software package for performing gapped alignments against the reference genome, DESeq for detecting differential gene expression. The log-fold change and a noise filter of minimum number of FPKM for a gene were used to identify differentiated genes. The complete data set was uploaded in the GEO repository, accession #ref. The lowest sum value had the lowest rank, which inversely correlated with the most significant gene expression. MATLAB was used for heat map creation with gene-wise hierarchical clustering. Average linkage and Euclidean distances were calculated unsupervised. Two-way ANOVA analysis over all genes indicated statistically significant variations in expression patterns. Comprehensive bioinformatics analysis was used to enrich the dataset for genes of interest including analysis of differential genes, series test of clusters, gene ontology, pathways, and gene co-expression networks.

Author contributions

Conceptualization, C.L., D.C., S.H., H.Z. and N.A.B.; Methodology, C.L., S.B., D.C. and R.C.; Formal Analysis, C.L., Z.L. and S.B.; Investigation, C.L., D.C., R.C., A.F. and S.B.; Data Curation, S.B.; Writing – Original Draft Preparation, C.L. and S.B.; Writing – Review & Editing, H.Z. and N.A.B.; Visualization, S.B.; Supervision, N.A.B.; Funding Acquisition, C.L., H.Z. and N.A.B.

Supplementary materials

Supplementary material associated with this article can be found, in the online version, at doi:10.1016/j.neo.2020.11.012.

References

[1] Argiris A, Karamouzis MV, Raben D, Ferris RL. Head and neck cancer. *Lancet* 2008;**371**:1695–709.

[2] Leemans CR, Braakhuis BJ, Brakenhoff RH. The molecular biology of head and neck cancer. *Nat Rev Cancer* 2011;**11**:9–22.

[3] Argiris A, Eng C. Epidemiology, staging, and screening of head and neck cancer. *Cancer Treat Res* 2003;**114**:15–60.

[4] Ragin CC, Modugno F, Gollin SM. The epidemiology and risk factors of head and neck cancer: A focus on human papillomavirus. *J Dent Res* 2007;**86**:104–14.

[5] Choi S, Myers JN. Molecular pathogenesis of oral squamous cell carcinoma: Implications for therapy. *J Dent Res* 2008;**87**:14–32.

[6] Syrigos KN, Karachalios D, Karapanagiotou EM, Nutting CM, Manolopoulos L, Harrington KJ. Head and neck cancer in the elderly: An overview on the treatment modalities. *Cancer Treat Rev* 2009;**35**:237–45.

[7] Kim Y, Okuyama K, Michi Y, Ohyama Y, Uzawa N, Yamaguchi S. Potential factors influencing the development of oral tongue squamous cell carcinoma in young mature patients: Lingual position of the mandibular second molar and narrow tongue space. *Oncol Lett* 2017;**14**:7339–43.

[8] Prince A, Aguirre-Ghizo J, Genden E, Posner M, Sikora A. Head and neck squamous cell carcinoma: New translational therapies. *Mt Sinai J Med* 2010;**77**:684–99.

[9] Vargas-Ferreira F, Nedel F, Etges A, Gomes AP, Furuse C, Tarquinio SB. Etiologic factors associated with oral squamous cell carcinoma in non-smokers and non-alcoholic drinkers: A brief approach. *Braz Dent J* 2012;**23**:586–90.

[10] Han MW, Lee JC, Kim YM, Cha HJ, Roh JL, Choi SH, Nam SY, Cho KJ, Kim SW, et al. Epithelial-mesenchymal transition: Clinical implications for nodal metastasis and prognosis of tongue cancer. *Otolaryngol Head Neck Surg* 2015;**152**:80–6.

[11] Patel DM, Shah J, Srivastava AS. Therapeutic potential of mesenchymal stem cells in regenerative medicine. *Stem Cells Int* 2013:496218.

[12] Satija NK, Singh VK, Verma YK, Gupta P, Sharma S, Afrin F, Sharma M, Sharma P, Tripathi RP, et al. Mesenchymal stem cell-based therapy: A new paradigm in regenerative medicine. *J Cell Mol Med* 2009;**13**:4385–402.

[13] Loebinger MR, Eddaoudi A, Davies D, Janes SM. Mesenchymal stem cell delivery of trail can eliminate metastatic cancer. *Cancer Res* 2009;**69**:4134–42.

[14] Studeny M, Marini FC, Dembinski JL, Zompetta C, Cabreira-Hansen M, Bekele BN, Champlin RE, Andreeff M. Mesenchymal stem cells: Potential precursors for tumor stroma and targeted-delivery vehicles for anticancer agents. *J Natl Cancer Inst* 2004;**96**:1593–603.

[15] Waterman RS, Morgenweck J, Nossaman BD, Scandurro AE, Scandurro SA, Betancourt AM. Anti-inflammatory mesenchymal stem cells (msc2) attenuate symptoms of painful diabetic peripheral neuropathy. *Stem Cells Transl Med* 2012;**1**:557–65.

[16] Brower V. Search and destroy: Recent research exploits adult stem cells' attraction to cancer. *J Natl Cancer Inst* 2005;**97**:414–16.

[17] Robertazzi A, Vargiu AV, Magistrato A, Ruggerone P, Carloni P, de Hoog P, Reedijk J. Copper-1,10-phenanthroline complexes binding to DNA: Structural predictions from molecular simulations. *J Phys Chem B* 2009;**113**:10881–90.

[18] Djouad F, Plence P, Bony C, Tropel P, Apparailly F, Sany J, Noel D, Jorgensen C. Immunosuppressive effect of mesenchymal stem cells favors tumor growth in allogeneic animals. *Blood* 2003;**102**:3837–44.

[19] Kidd S, Spaeth E, Dembinski JL, Dietrich M, Watson K, Klopp A, Battula VL, Weil M, Andreeff M, et al. Direct evidence of mesenchymal stem cell tropism for tumor and wounding microenvironments using in vivo bioluminescent imaging. *Stem Cells* 2009;**27**:2614–23.

[20] Yang B, Wu X, Mao Y, Bao W, Gao L, Zhou P, Xie R, Zhou L, Zhu J. Dual-targeted antitumor effects against brainstem glioma by intravenous delivery of tumor necrosis factor-related, apoptosis-inducing, ligand-engineered human mesenchymal stem cells. *Neurosurgery* 2009;**65**:610–24.

[21] Nakamizo A, Marini F, Amano T, Khan A, Studeny M, Gumin J, Chen J, Hentschel S, Vecil G, et al. Human bone marrow-derived mesenchymal stem cells in the treatment of gliomas. *Cancer Res* 2005;**65**:3307–18.

[22] Norozi F, Ahmadzadeh A, Shahrabi S, Vosoughi T, Saki N. Mesenchymal stem cells as a double-edged sword in suppression or progression of solid tumor cells. *Tumour Biol* 2016;**37**:11679–89.

[23] Ohlsson LB, Varas L, Kjellman C, Edvardsen K, Lindvall M. Mesenchymal progenitor cell-mediated inhibition of tumor growth in vivo and in vitro in gelatin matrix. *Exp Mol Pathol* 2003;**75**:248–55.

[24] Khakoo AY, Pati S, Anderson SA, Reid W, Elshal MF, Rovira II, Nguyen AT, Malide D, Combs CA, et al. Human mesenchymal stem cells exert potent antitumorigenic effects in a model of kaposi's sarcoma. *J Exp Med* 2006;**203**:1235–47.

[25] Li GC, Ye QH, Dong QZ, Ren N, Jia HL, Qin LX. Mesenchymal stem cells seldomly fuse with hepatocellular carcinoma cells and are mainly distributed in the tumor stroma in mouse models. *Oncol Rep* 2013;**29**:713–19.

[26] Rappa G, Mercapide J, Lorico A. Spontaneous formation of tumorigenic hybrids between breast cancer and multipotent stromal cells is a source of tumor heterogeneity. *Am J Pathol* 2012;**180**:2504–15.

[27] Wang Y, Fan H, Zhou B, Ju Z, Yu L, Guo L, Han J, Lu S. Fusion of human umbilical cord mesenchymal stem cells with esophageal carcinoma cells inhibits the tumorigenicity of esophageal carcinoma cells. *Int J Oncol* 2012;**40**:370–7.

[28] Placencio VR, Li X, Sherrill TP, Fritz G, Bhowmick NA. Bone marrow derived mesenchymal stem cells incorporate into the prostate during regrowth. *PloS One* 2010;**5**:e12920.

[29] Valencia T, Kim JY, Abu-Baker S, Moscat-Pardos J, Ahn CS, Reina-Campos M, Duran A, Castilla EA, Metallo CM, et al. Metabolic reprogramming of stromal fibroblasts through p62-mtorc1 signaling promotes inflammation and tumorigenesis. *Cancer Cell* 2014;**26**:121–35.

[30] Hong D, Fritz AJ, Zaidi SK, van Wijnen AJ, Nickerson JA, Imbalzano AN, Lian JB, Stein JL, Stein GS. Epithelial-to-mesenchymal transition and cancer stem cells contribute to breast cancer heterogeneity. *J Cell Physiol* 2018;**233**:9136–44.

[31] Mallini P, Lennard T, Kirby J, Meeson A. Epithelial-to-mesenchymal transition: What is the impact on breast cancer stem cells and drug resistance. *Cancer Treat Rev* 2014;**40**:341–8.

[32] Melzer C, von der Ohe J, Hass R. Involvement of actin cytoskeletal components in breast cancer cell fusion with human mesenchymal stroma/stem-like cells. *Int J Mol Sci* 2019;**20**:876–89.

[33] Salgado AJ, Reis RL, Sousa NJ, Gimble JM. Adipose tissue derived stem cells secretome: Soluble factors and their roles in regenerative medicine. *Curr Stem Cell Res Ther* 2010;**5**:103–10.

[34] Wynn RF, Hart CA, Corradi-Perini C, O'Neill L, Evans CA, Wraith JE, Fairbairn LJ, Bellantuono I. A small proportion of mesenchymal stem cells strongly expresses functionally active cxcr4 receptor capable of promoting migration to bone marrow. *Blood* 2004;**104**:2643–5.

[35] Xu WT, Bian ZY, Fan QM, Li G, Tang TT. Human mesenchymal stem cells (hmscs) target osteosarcoma and promote its growth and pulmonary metastasis. *Cancer Lett* 2009;**281**:32–41.

[36] Liotta F, Querci V, Mannelli G, Santarlasci V, Maggi L, Capone M, Rossi MC, Mazzoni A, Cosmi L, et al. Mesenchymal stem cells are enriched in head neck squamous cell carcinoma, correlates with tumour size and inhibit t-cell proliferation. *Br J Cancer* 2015;**112**:745–54.

[37] Song JY, Kang HJ, Ju HM, Park A, Park H, Hong JS, Kim CJ, Shim JY, Yu J, et al. Umbilical cord-derived mesenchymal stem cell extracts ameliorate atopic dermatitis in mice by reducing the t cell responses. *Sci Rep* 2019;**9**:6623.

[38] Gast CE, Silk AD, Zarour L, Riegler L, Burkhart JG, Gustafson KT, Parappilly MS, Roh-Johnson M, Goodman JR, et al. Cell fusion potentiates tumor heterogeneity and reveals circulating hybrid cells that correlate with stage and survival. *Sci Adv* 2018;**4**:7828.

[39] Rizvi AZ, Swain JR, Davies PS, Bailey AS, Decker AD, Willenbring H, Grompe M, Fleming WH, Wong MH. Bone marrow-derived cells fuse with normal and transformed intestinal stem cells. *Proc Natl Acad Sci U S A* 2006;**103**:6321–5.

[40] Sahai E, Astsaturov I, Cukierman E, DeNardo DG, Egeblad M, Evans RM, Fearon D, Greten FR, Hingorani SR, et al. A framework for advancing our understanding of cancer-associated fibroblasts. *Nat Rev Cancer* 2020;**20**:174–86.

[41] Hayward SW, Wang Y, Cao M, Hom YK, Zhang B, Grossfeld GD, Sudilovsky D, Cunha GR. Malignant transformation in a nontumorigenic human prostatic epithelial cell line. *Cancer Res* 2001;**61**:8135–42.

[42] Olumi AF, Grossfeld GD, Hayward SW, Carroll PR, Tlsty TD, Cunha GR. Carcinoma-associated fibroblasts direct tumor progression of initiated human prostatic epithelium. *Cancer Res* 1999;**59**:5002–11.

[43] Kato M, Placencio-Hickok VR, Madhav A, Haldar S, Tripathi M, Billet S, Mishra R, Smith B, Rohena-Rivera K, et al. Heterogeneous cancer-associated fibroblast population potentiates neuroendocrine differentiation and castrate resistance in a cd105-dependent manner. *Oncogene* 2019;**38**:716–30.

[44] Wu YL, Li HY, Zhao XP, Jiao JY, Tang DX, Yan LJ, Wan Q, Pan CB. Mesenchymal stem cell-derived ccn2 promotes the proliferation, migration and invasion of human tongue squamous cell carcinoma cells. *Cancer Sci* 2017;**108**:897–909.

[45] Thomas C, Karnoub AE. Lysyl oxidase at the crossroads of mesenchymal stem cells and epithelial-mesenchymal transition. *Oncotarget* 2013;**4**:376–7.

[46] Tanabe S, Aoyagi K, Yokozaki H, Sasaki H. Regulated genes in mesenchymal stem cells and gastric cancer. *World J Stem Cells* 2015;**7**:208–22.

[47] Zhou S, Cecere R, Philip A. Cd109 released from human bone marrow mesenchymal stem cells attenuates tgf-beta-induced epithelial to mesenchymal transition and stemness of squamous cell carcinoma. *Oncotarget* 2017;**8**:95632–47.

[48] Jung Y, Kim JK, Shiozawa Y, Wang J, Mishra A, Joseph J, Berry JE, McGee S, Lee E, et al. Recruitment of mesenchymal stem cells into prostate tumours promotes metastasis. *Nat Commun* 2013;**4**:1795.

[49] Salo S, Bitu C, Merkku K, Nyberg P, Bello IO, Vuoristo J, Sutinen M, Vahanikkila H, Costea DE, et al. Human bone marrow mesenchymal stem cells induce collagen production and tongue cancer invasion. *PLoS One* 2013;**8**:e77692.

[50] De Boeck A, Pauwels P, Hensen K, Rummens JL, Westbroek W, Hendrix A, Maynard D, Denys H, Lambein K, et al. Bone marrow-derived mesenchymal stem cells promote colorectal cancer progression through paracrine neuregulin 1/her3 signalling. *Gut* 2013;**62**:550–60.

[51] Houthuijzen JM, Daenen LG, Roodhart JM, Voest EE. The role of mesenchymal stem cells in anti-cancer drug resistance and tumour progression. *Br J Cancer* 2012;**106**:1901–6.

[52] Bergfeld SA, Blavier L, DeClerck YA. Bone marrow-derived mesenchymal stromal cells promote survival and drug resistance in tumor cells. *Mol Cancer Ther* 2014;**13**:962–75.

[53] Ji N, Yu JW, Ni XC, Wu JG, Wang SL, Jiang BJ. Bone marrow-derived mesenchymal stem cells increase drug resistance in cd133-expressing gastric cancer cells by regulating the pi3k/akt pathway. *Tumour Biol* 2016;**37**:14637–51.

[54] Ji R, Zhang B, Zhang X, Xue J, Yuan X, Yan Y, Wang M, Zhu W, Qian H, et al. Exosomes derived from human mesenchymal stem cells confer drug resistance in gastric cancer. *Cell Cycle* 2015;**14**:2473–83.